Atmospheric
Chemistry
and Physics

Supplement of

Measurement report: Black carbon properties and concentrations in southern Sweden urban and rural air – the importance of long-range transport

Erik Ahlberg et al.

Correspondence to: Erik Ahlberg (erik.ahlberg@nuclear.lu.se) and Axel Eriksson (axel.eriksson@design.lth.se)

Supplement

On the use of "dual vaporizer" in the SP-AMS measurements

When engaging the laser there is a small increase in the "Organic" signal due to vaporization of non-refractory components. Additionally, all species signals increase ~10% due to increased sensitivity with dual vaporizers. The increased sensitivity is partly due to increased collection efficiency for absorbing particles, predominantly BC containing particles, which produce additional vapor passing the laser beam. However, sensitivity is also increased by impaction of bounced particles (which may or may not absorb at 1064 nm) on surfaces heated by the laser. These effects are not presently constrained. Compounding the difficulty of constraining them is the fact that vapor temperature is variable. Hence, we cannot currently interpret the ratios in Table S1. in terms of soot coating composition. While the "laser of" data is normally used for non-refractory-PM analysis to avoid the caveats mentioned above, a minor instrumental malfunction prevents this approach in the present study. Hence we have used "laser on" data for both datasets. However, as shown in Table S1, this does not significantly affect our results

HOA mass spectra

The plume MS was calculated using a background subtraction procedure similar to a recent study of ship plumes in the region (Ausmeel et al., 2019) and includes 90 traffic exhaust plumes. In Figure S9, two other traffic OA, or hydrocarbon-like OA (HOA), obtained in Barcelona, by Mohr et al. (2012) , and in Paris, by Crippa et al. (2013), are shown for comparison. These HOA mass spectra are now routinely used as input for OA source apportionment

using positive matrix factorization (PMF) with the multilinear engine (ME-2) on aerosol mass spectrometer (AMS) data (Crippa et al., 2014). A growing number of studies in Europe and beyond use HOA mass spectral patterns to constrain traffic contributions to OA. Hence, detailed comparison of HOA MS could potentially benefit future source apportionment efforts. While there is a striking similarity between the Malmö, Paris and Barcelona HOA profiles, there are noteworthy differences. To compare these mass spectra we use θ angles (Kostenidou et al., 2009). Briefly, θ angles up to 15° indicates a great match between two spectra. θ from 16° to 30° could indicate different sources with some limited similarities while θ from 31° suggests that spectra are significantly different. In our study, the Malmö HOA profile is found to be more similar to the Paris HOA ($\theta = 13.8°$). Meantime, the Barcelona HOA shows slightly worse overlap with HOA from our study ($\theta = 18.0°$). The Malmö data show near unity ratios of m/z's 41/43, and 55/57. For the Paris and Barcelona data m/z 41 < m/z 43 and m/z 55 < m/z 57. In fact, the 55/57 ratio is used to differentiate HOA from cooking OA, which gives a lower ratio of 55/57 than HOA. However, considering the plume background employed, we do not consider cooking OA influence in Malmö a likely explanation for this difference. We tentatively attribute it to differences in the vehicle fleet, geographical and/or temporal. Another noteworthy difference is the inclusion of m/z 39 in the mass spectra from Malmö and Barcelona, but not Paris. The organic signal at m/z 39 suffers from interferences from thermally ionized potassium, which normally prevents m/z 39 from being used in unit mass resolution datasets. In high-resolution datasets (all three HOA MS discussed here where recorded with high resolution) the separation of potassium and organic signal is normally unambiguous. Hence, source apportionment based on high-resolution data should not omit m/z 39.

Table S1. Slopes between SP-AMS species concentrations using Laser On vs Laser Off configuration.

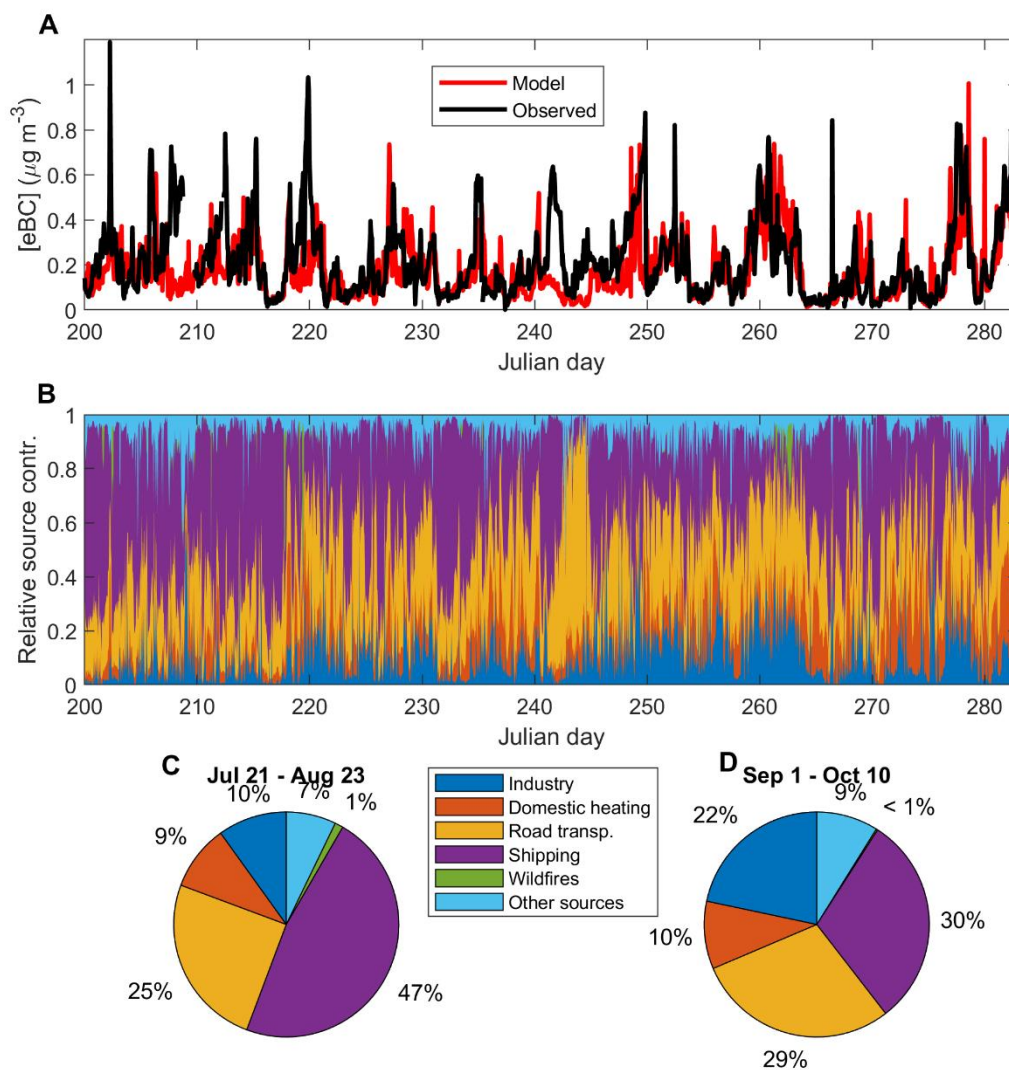| Species	Urban slope $\pm 1\sigma$ (r^2)	Rural slope $\pm 1\sigma$ (r^2)
Organics	1.17 ± 0.016 (0.91)	1.21 ± 0.020 (0.78)
Nitrate	1.09 ± 0.008 (0.97)	1.07 ± 0.003 (0.99)
Sulphate	1.09 ± 0.005 (0.99)	1.05 ± 0.007 (0.95)
Ammonium	1.07 ± 0.007 (0.98)	1.07 ± 0.007 (0.96)
Chloride	1.14 ± 0.010 (0.96)	1.12 ± 0.005 (0.97)

Figure S1. Modelled BC and measured eBC concentrations at the rural site during both campaigns (panel A), and modelled sources (panel B) using CAMS emission data and ADCHEM. Pie charts show the sources during the respective campaigns.
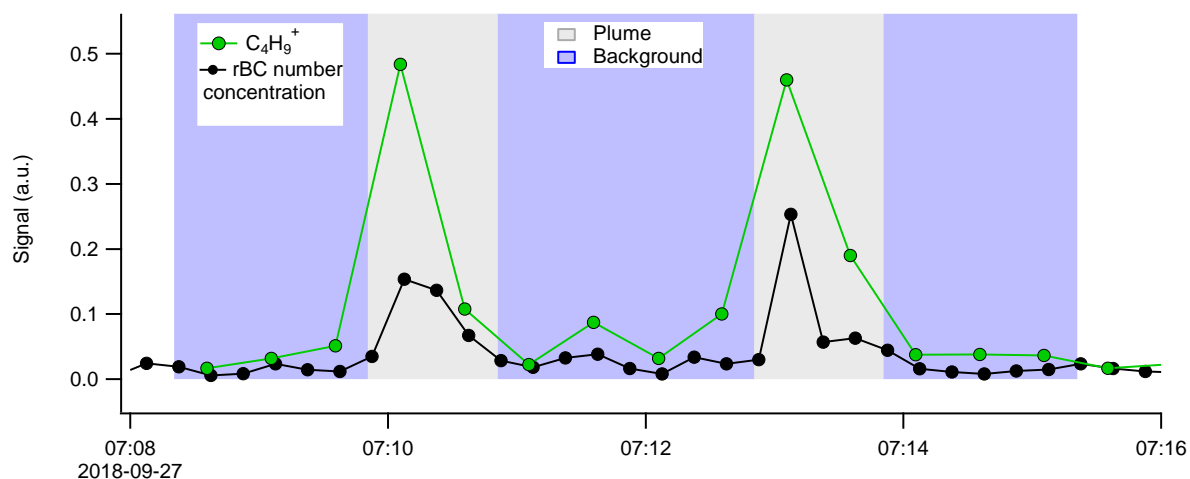
60

Figure S2. An example of typical plumes of rBC number concentration (measured by SP2) and the HOA proxy mass fragment C4H9+ (measured by SP-AMS). Plume mass spectra were isolated by subtracting the mass spectra of the background before and after the plumes.
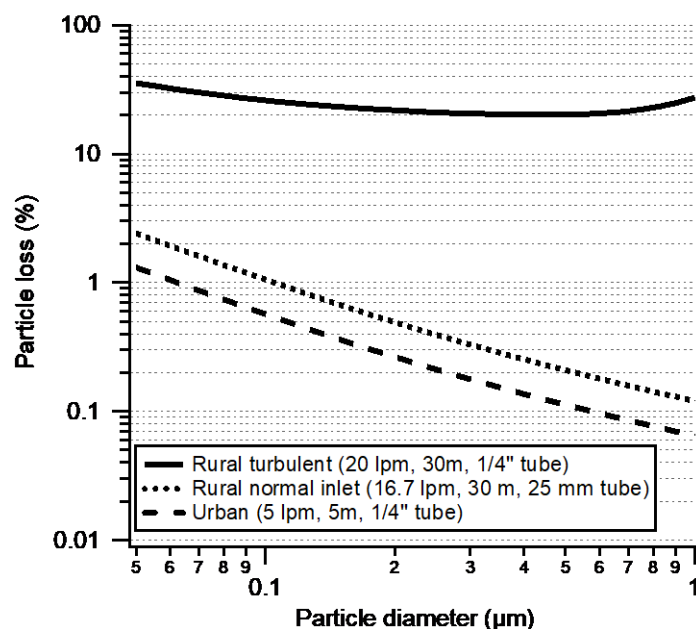

Figure S3. Calculated losses in the longest tube sections during urban and rural campaigns.
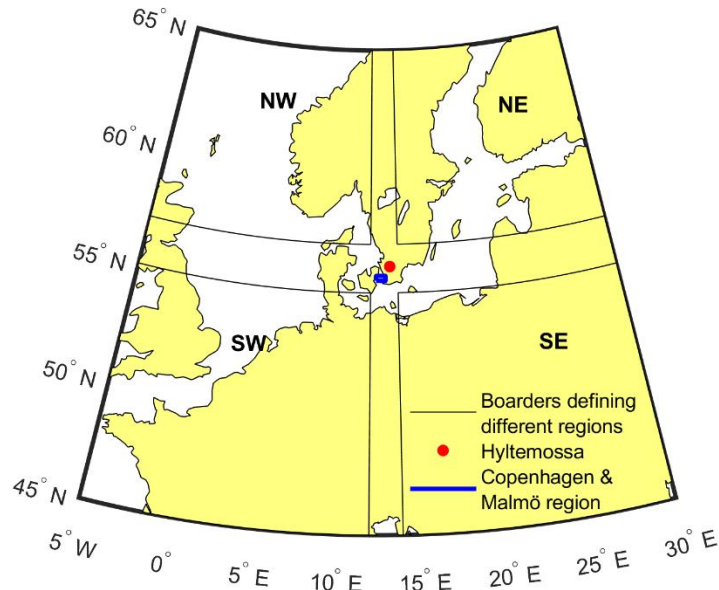
Figure S4. Map illustrating the definition of the different regions of air mass origin relative to the Hyltemossa field station. NW (Lat>57°, Lon<12°), NE (Lat>57°, Lon>14°), SE (Lat<55°, Lon>14°), SW (Lat<55°, Lon<12°) and Copenhagen and Malmö region (Lat>55.5°, Lat<55.7°, Lon>12.4°, Lon<13.1°)

Table S2. Median eBC concentrations and percentage of time (values within parenthesis) with existing observations of different eBC subsets based on air mass origin and cumulative precipitation during the last 48 hours upwind Hyltemossa. The results are from the entire year of 2018. The total Aethalometer data coverage was 99.4 %.

Source region(s)	[eBC/(ng m^{-3})]	[eBC/(ng m^{-3})], <1 mm precip.
SE	563.0 (19.7)	571 (15.1)
NE	149.9 (22.4)	156.1 (14.2)
NW	101.2 (23.2)	118.9 (12.4)
SW	192.0 (27.7)	288.2 (12.0)
Without CPH/Malmö	187.0 (87.7)	226.9 (53.4)
With CPH/Malmö	185.7 (11.7)	354.7 (5.2)
SW without CPH/Malmö	187.1 (20.5)	265.2 (9.4)
SW with CPH/Malmö	206.6 (7.1)	370.0 (2.7)
All	187.0 (99.4)	235.2 (0.586)

Table S3. p-values for two-sided rank sum tests of the hypothesis that eBC concentration subsets come from distributions with equal medians. p-values<0.001 are denoted with *.**

	SE	NE	NW	SW	SW no CPH or Malmö	SW with CPH or Malmö	All
SE	1.0	***	***	***	***	***	***
NE	***	1.0	***	***	***	***	***
NW	***	***	1.0	***	***	***	***
SW	***	***	***	1.0	0.184	0.008	0.456
SW no CPH or Malmö	***	***	***	0.184	1.0	***	0.482
SW with CPH or Malmö	***	***	***	0.008	***	1.0	0.004
All	***	***	***	0.456	0.482	0.004	1.0

Table S4. p-values for two-sided rank sum tests of the hypothesis that eBC concentration subsets come from distributions with equal medians. Same as Table S2 but only considering conditions with < 1 mm precipitation during the last 48 hours upwind Hyltemossa. p-values<0.001 are denoted with ***.

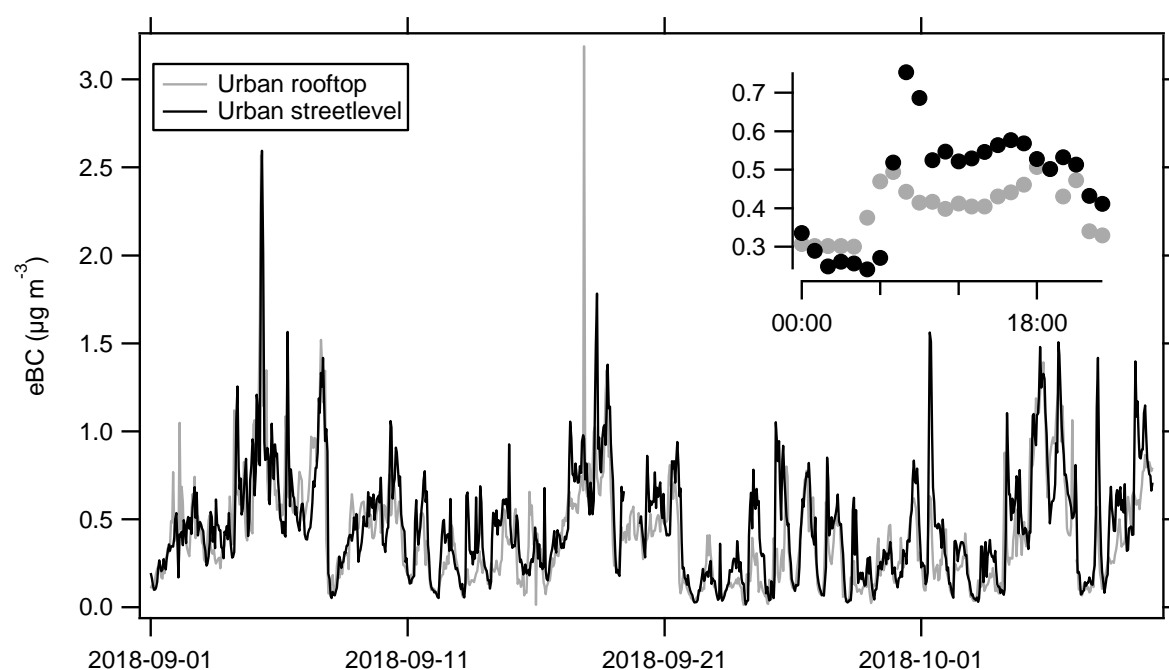|	SE	NE	NW	SW	SW no CPH or Malmö	SW with CPH or Malmö	All
SE	1.0	***	***	***	***	***	***
NE	***	1.0	***	***	***	***	***
NW	***	***	1.0	***	***	***	***
SW	***	***	***	1.0	0.017	***	***
SW no CPH or Malmö	***	***	***	0.017	1.0	***	0.028
SW with CPH or Malmö	***	***	***	***	***	1.0	***
All	***	***	***	***	0.028	***	1.0

90

Figure S5. Time-series showing a comparison between the urban street and roof-top measurements. Insert shows the average diurnal cycles during the measurement campaign.
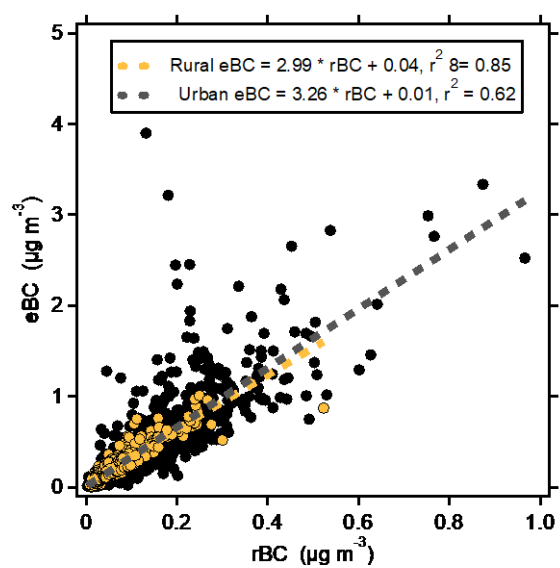
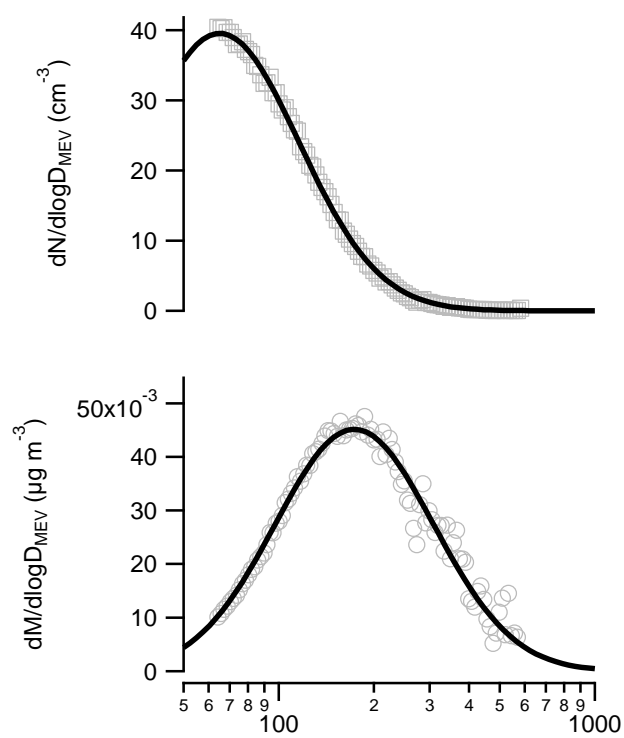**Figure S6. Correlation between 1h averages of Aethalometer (eBC) and SP2 (rBC) data.**

95

Figure S7. Size distribution and lognormal fit example for 24 h data at the rural site.
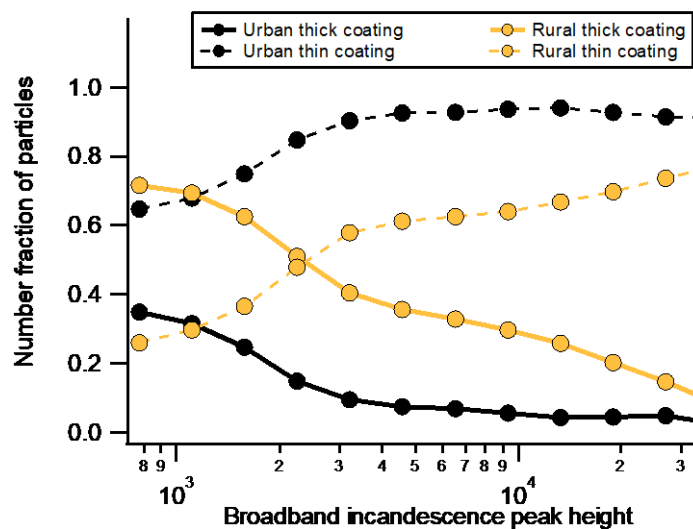
Figure S8. Example of the coating thickness from the delay-time method showing the number fraction of thinly/thickly coated BC particles as a function of the incandescence signal (rBC core mass).
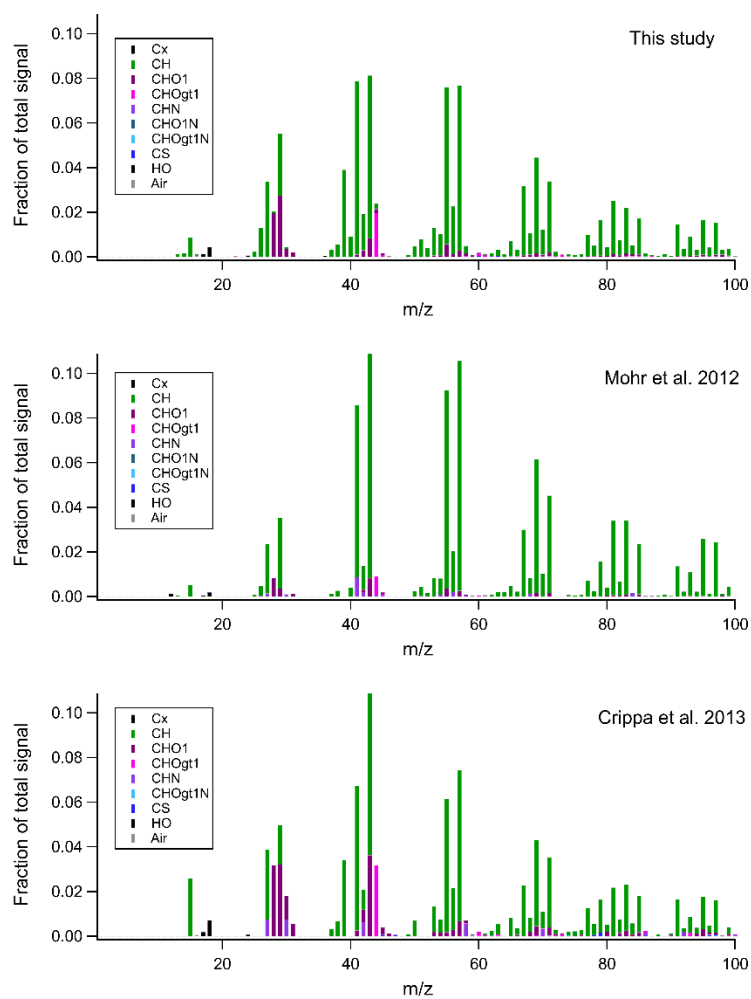

Figure S9. Mass spectra showing the traffic aerosol peaks from this study (top) in comparison with two other studies.